Effect of surface treatment on the spot weldability of Fe–Mn–Al–Cr alloys

C. J. LIN, M. T. LIAO
National Yuen Lin Institute of Polytechnology, Yuen-Lin, Taiwan

J. G. DUH
Department of Material Science and Engineering, National Tsing Hua University, Hsin-Chu, Taiwan

An Fe–26.3Mn–6.8Al–5.5Cr–0.9Mo–1.0C alloy was employed to study spot weldability. A series of Lobe curves was obtained under various welding conditions including electrode force, weld current, weld time and hold time. The acceptable weld currents ranged from 3.5–6kA, which is narrower than those of HSLA and plain carbon steel. The effect of surface treatment on the weldability of this alloy system was investigated. For an untreated specimen with α-Al_2O_3 layer on the surface, the Lobe curve exhibits a narrower range than those of surface acid-pickled specimens. In addition, for the surface untreated specimen, the plug size was linearly proportional to the weld time. However, for the surface acid-pickled specimen, the degree of dependence of plug size on the weld time decreased as the electrode force increased. It was also observed that the indentation was proportional to the weld current for this alloy system. The dependence of indentation on the weld time was influenced by both the surface condition and the electrode force.

1. Introduction

The Fe–Mn–Al-based alloy system has attracted a great deal of research attention owing to its potential as a substitute for conventional Fe–Ni–Cr stainless steel. The combination of manganese and carbon acts as the austenitic stabilizer which extends and stabilizes the gamma loop in iron and then retains the face-centred cubic austenitic phase [1–3]. Recently, research concerning the development of the Fe–Mn–Al system has been carried out by our group, which included the effect of carbon and chromium on high-temperature oxidation behaviour, the oxidation-induced phase transformation, and the nitriding kinetics [4–11]. The results provide promising potential for Fe–Mn–Al-based alloy to substitute the conventional Fe–Ni–Cr system. However, if the newly developed Fe–Mn–Al alloys are to be used in practical application the weldability must be assessed. To date, there has been little research on the weldability of Fe–Mn–Al alloy. Chou and co-workers [12–14] examined an Fe–29% Mn–8% Al–x% C ($x = 0.5, 0.8, 1.1$) alloys in which the gas tungsten arc (GTA) weld metal by U-bend and tensile tests exhibited excellent strength (>900 MPa) and ductility (>20%). They also observed that the carbon content cast a strong influence on the residual ferrite. The purpose of the present work was to investigate further the effect of surface treatment on the weldability of this alloy system. The relations between the weld time, weld current and plug size were studied and are discussed.

2. Experimental procedure

The specimen was prepared from pure aluminium, manganese, chromium and iron raw materials in an induction furnace and cast into a 1500 kg mould. The ingot was solution treated at 1150 °C for 4 h and then hot rolled 20–30 times at 1150 °C to a final thickness of 3.5 mm. The reduction percentage per hot roll pass was about 20%. It was then cold rolled into a 1 mm thickness sheet, and bright annealing took place at 1175 °C for 30 min under a hydrogen reduction atmosphere. A portion of the annealed cold-rolled plate was cut into a 30 mm × 100 mm size for the spot-weld specimen and designated Specimen A. Another annealed sheet was acid pickled with 15% HNO_3 plus 1% HF aqueous solution to remove the surface scale, and was cut into a 30 mm × 100 mm size, Specimen B. The chemical composition for the alloy in this study is listed in Table I.

Both Specimens A and B were first phase identified by X-ray diffraction. All the specimens were spot welded in an ND-50-46 spot-weld machine (Dengensha, Japan) at 220 V, 60 Hz, maximum current 20 000A with a truncated CF type electrode tip as shown in Fig. 1a. The controlling experimental parameters included electrode force, weld current, and weld time. The spot-welded position and welded specimen size are shown in Fig. 1b, in which a single spot test piece was applied according to the JIS Z3136 specification [15]. These spot-welded specimens were peel-tested as shown in Fig. 2a [16]. The knife-edged caliper was used to measure the button size as shown

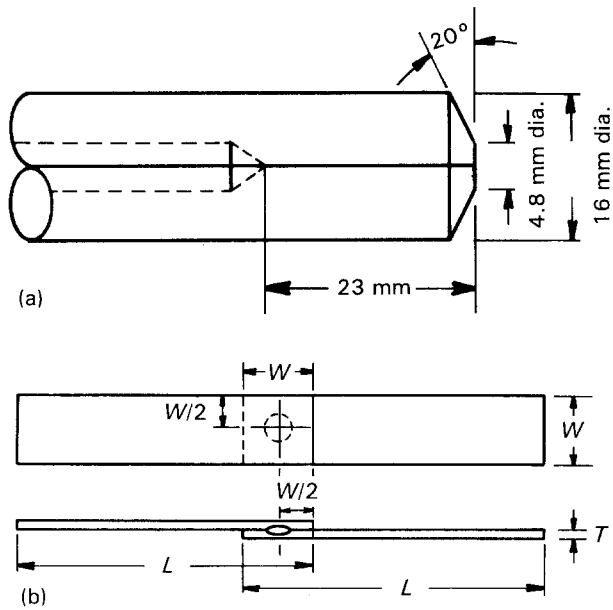| Mn	Al	Cr	Mo	Si	C	Fe
26.3	6.8	5.5	0.9	0.4	1.0	Bal.

(a)

(b)

Figure 1 (a) The shape of the electrode tip. (b) Shape and dimensions of the test piece. $W = 30$ mm, $L = 100$ mm, $T = 1.0$ mm.
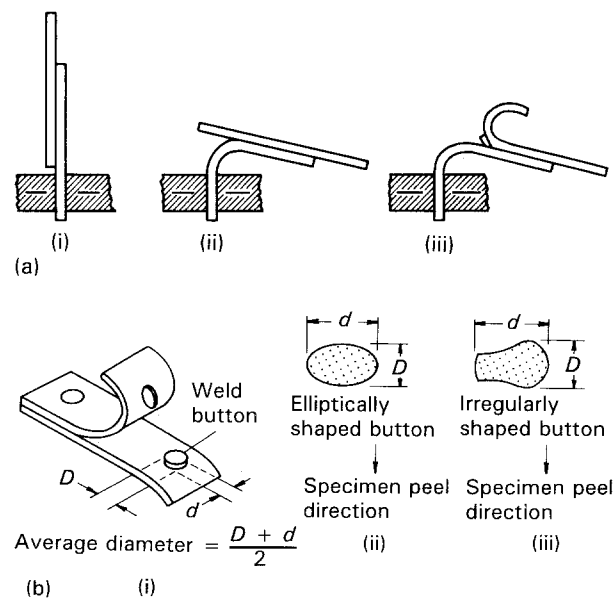

Figure 2 (a) Diagrammatic representation of the process of the peel test. (b) Schematic diagram of the measurement of nugget size.

in Fig. 2b. The plug size is the average diameter and equal to $(d + D)/2$ [17], where d and D are the measured lengths of the plug in the perpendicular direction. The indentation was measured with a dial gauge to obtain the height difference between the joint, such as the centre of the dent, and the sheet surface at a point of about one dent diameter distance from the centre of the dent, which is in accordance with Grade CF of JIS Z3140 [18].

3. Results and discussion

The peel test is one of the most widely used methods to describe the spot weldability. Early reports pointed out that plain carbon steel spot welds with pull-out or button-type fracture on peeling would exhibit satisfactory mechanical properties [19, 20]. Owing to ease of operation associated with available mechanical evaluation, the peel test suffices to act as an appropriate quality-control criterion. Sawhill [21] reported that the peel test could be applied to automotive
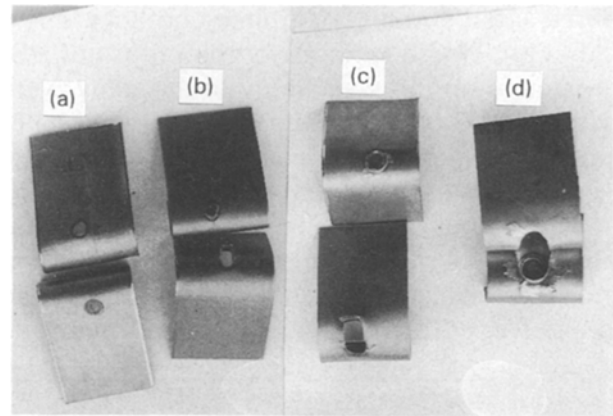

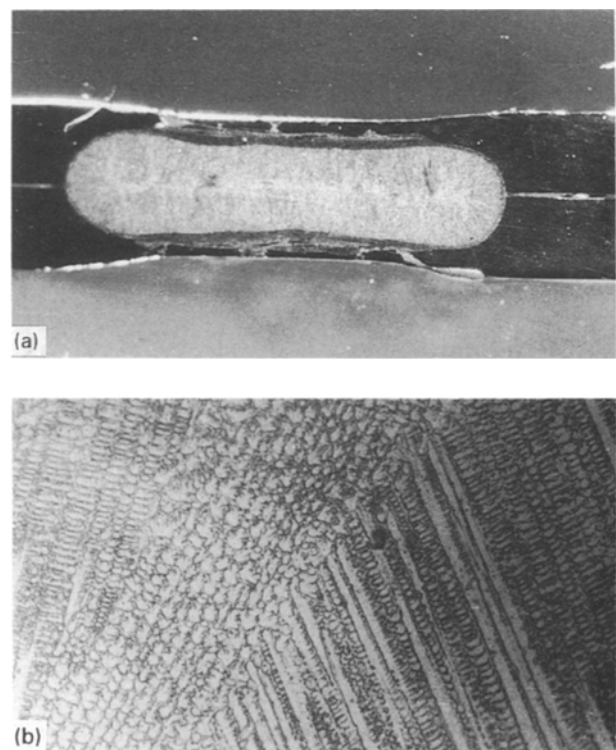*Figure 3* The failure mode of Specimen B after the peel test.

Figure 4 (a) Optical micrograph showing the nugget of Specimen A under 210 kgf electrode force, 15 cycles weld time, 4.6 kA weld current and 30 cycles hold time. (b) Optical micrograph showing the dendritic structure inside the welded nugget for Specimen B under 210 kgf electrode force, 5 cycles weld time, 3.83 kA weld current and 30 cycles hold time.

production and service performance of high-strength steel. In this study, the peel test is employed as the primary method to evaluate the weldability of this newly developed high-strength Fe–Mn–Al alloy.

The normal fracture surface of a spot-welded plug of Specimen B alloy is shown in Fig. 3. For a constant weld current with increasing weld time, the failure mode after the peel test will, in general, proceed from interface failure to button failure, then to pull-out failure and finally toward expulsive failure. Fig. 4a represents the cross-sectional view of a nugget of Specimen B under 210 kgf electrode force, 15 cycles weld time, 4.6 kA weld current and 30 cycles hold time. It should be pointed out that in Fig. 4a, the diameter of flat area in the spot weld is slightly smaller than 4.8 mm, the nominal contact diameter of the spot weld. The discrepancy is caused by the electrode-tip damage, which shrank due to successive welding. A detailed microstructure of the dendritic structure is shown in Fig. 4b. In the central portion of the weld pool, a typical equi-axed dendritic structure was found, as indicated in the central-to-left portion of Fig. 4b. However, away from the central region, the columnar dendritic structure was observed, as shown in the right portion of Fig. 4b. Tiller and Rutter [22] proposed a relationship between the solidification pattern and the temperature gradient of the weld metal. It is argued that in the central region of the weld, the temperature gradient is low, so equiaxed dendritic structure is formed. However, the temperature gradient is increased in the outer portion of the weld, and the columnar structure is thus favoured.

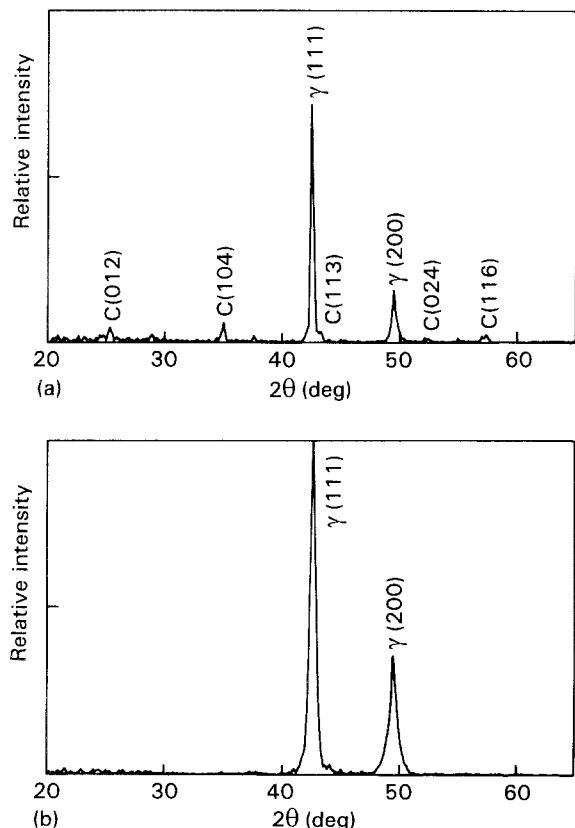Fig. 5a and b represent the X-ray diffraction patterns of Specimen A and B, respectively, before wel-

ding. The major phase is f c c structure for both specimens. The only difference between Fig. 5a and b is the presence of α-Al$_2$O$_3$ on Specimen A. As in our previous study [7, 9, 10], a layer of α-Al$_2$O$_3$ existed on Fe–Mn–Al–Cr alloy after high-temperature oxidation. In some applications of the Fe–Mn–Al–Cr system that do not require surface brightness, the alloy with α-Al$_2$O$_3$ on the surface can provide anti-oxidation resistance. In this study, α-Al$_2$O$_3$ was formed during the hot-rolling process for Specimen A. For Specimen B, the alloy was acid pickled and the surface

Figure 5 X-ray diffraction patterns for (a) Specimen A and (b) surface acid-pickled Specimen B, before spot welding.
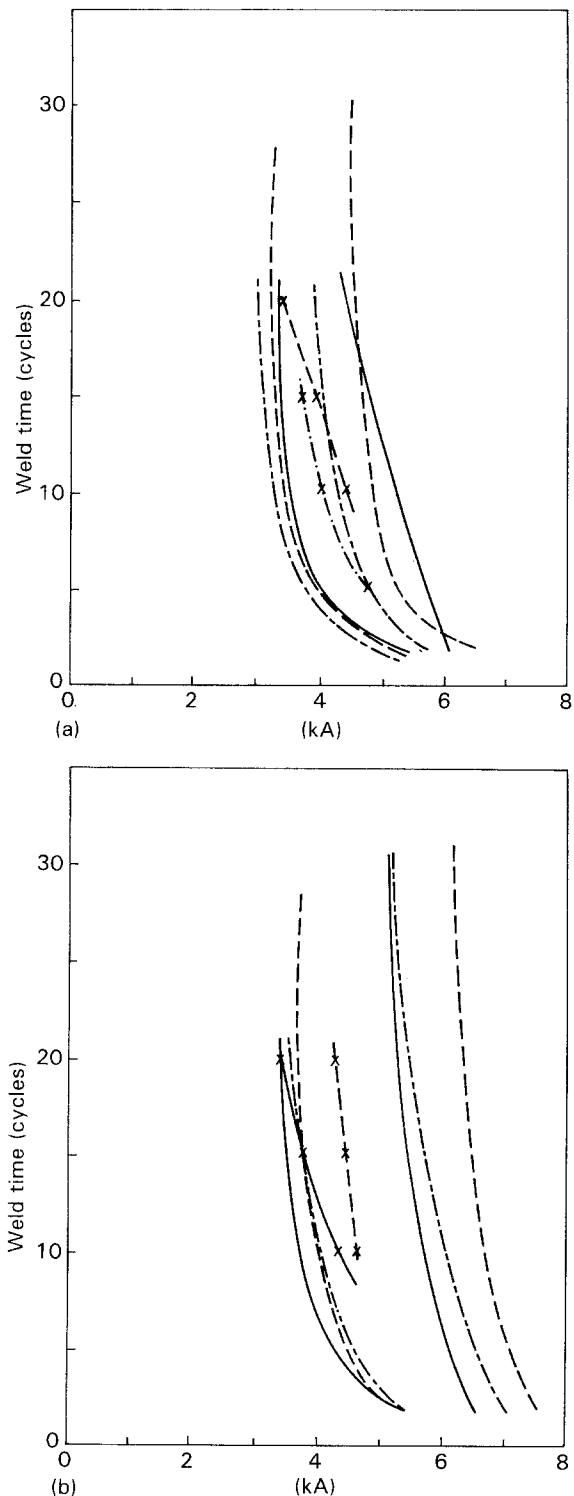

Figure 6 Lobe curves for (a) Specimen A and (b) Specimen B, under different electrode forces with hold time 30 cycles. (———) 150 kgf, (—·—) 210 kgf, (- - -) 290 kgf, (×) 4.8 mm plug size.

scale was then removed, so no layer of $\alpha\text{-Al}_2\text{O}_3$ was formed.

A series of Lobe curves was obtained with various welding conditions including electrode force, weld current, weld time and hold time. Fig. 6a and b show the Lobe curves for Specimens A and B, respectively. Expulsive failure will occur in the region beyond the upper part of the Lobe curve, which is considered to be unacceptable in practical welding. Likewise, interfacial failure takes place under the lower portion of the Lobe curve and is also unacceptable. Only welds made with appropriate currents and times lying within the Lobe curve are considered acceptable. From Fig. 6, it appears that the acceptable minimum weld current for Specimen A is somewhat lower than that for Specimen B. Specimen A contains an $\alpha\text{-Al}_2\text{O}_3$ layer on the surface which would, in turn, increase the contact resistance during welding. Consider the heat generated in the spot-welded region, i.e. $Q = I^2 Rt$, where I, t and R represent the weld current, weld time and contact resistance, respectively. Higher contact resistance, R, will introduce higher generating heat, so the maximum acceptable weld current for Specimen A is lower. From Fig. 6, it is also observed that the acid-pickled Specimen B exhibits larger weldable region, as compared to Specimen A. Also indicated in Fig. 6 are the measured data corresponding to a 4.8 mm full-sized weld. For Specimen A with higher contact resistance, the full size weld curve is located near the centre of the Lobe curve. However, for Specimen B with an acid-pickled surface, the full-size weld curve shifts towards the left side of the Lobe curve.

Fig. 7 indicates the welding Lobe diagram for high-strength low-alloy steel and plain carbon steel based on peel data in the literature [21], in which the weldable currents for HSLA steel and plain carbon steel ranges from 7–9 kA. However, the current ranges for Fe–Al–Mn–Cr alloy in this study are around
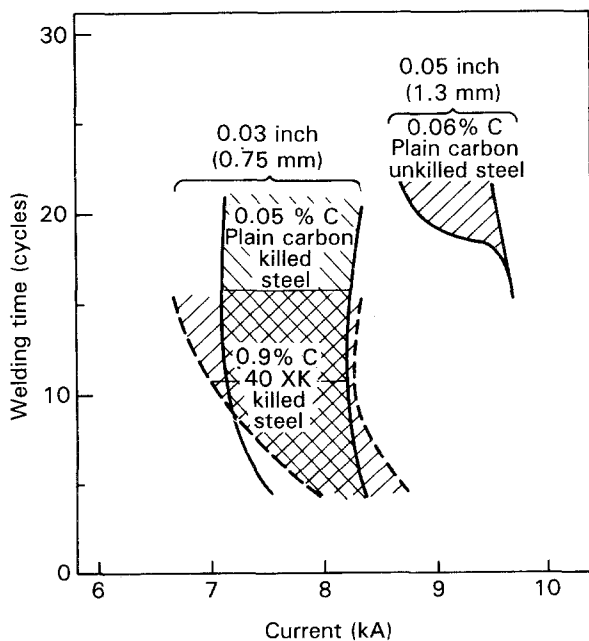
3.5–6 kA, as indicated in Fig. 6. It is apparent that the Fe–Al–Mn–Cr alloy can be welded at lower current, which is beneficial from the viewpoint of practical application.

The change of plug size under different surface conditions, weld time, electrode force, and weld current was also investigated. The relationship between plug size and weld time at different weld currents and surface conditions are shown in Figs 8 and 9. The acceptable Lobe region is indicated in these figures by solid lines. It appears that the plug size is proportional to the weld time within the Lobe region. Below the lower portion of Lobe curve, the plug size is, however, insufficient to be considered as acceptable. Relatively speaking, the dependence of plug size on weld time is more significant for Specimen A than that for Specimen B, because the slopes in Figs 8 and 9 are larger for Specimen A. For example, in the cases of Specimen B
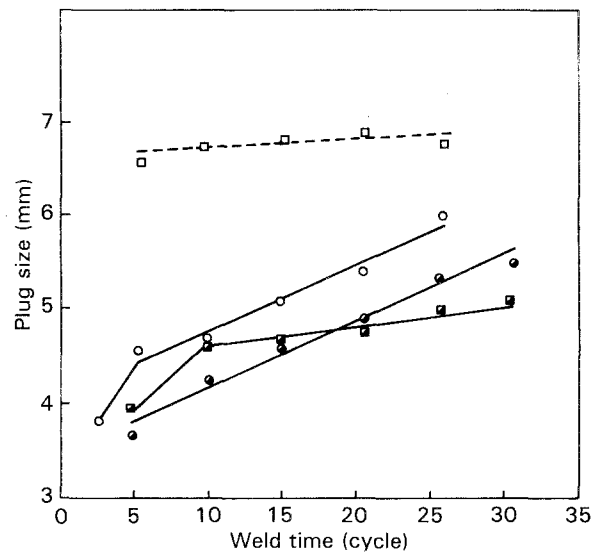

Figure 8 Plug size as a function of weld time at an electrode force of 290 kgf. (○) Specimen A, 4.34 kA; (◑) Specimen A, 3.4 kA, (□) Specimen B, 7.26 kA; (▣) Specimen B, 3.98 kA.
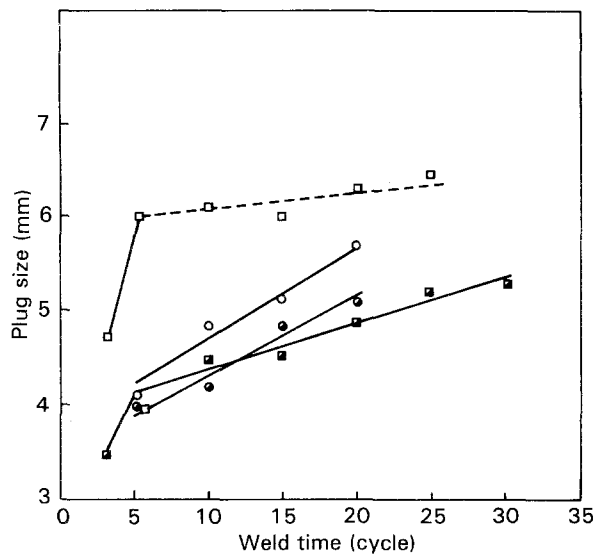

Figure 7 Welding lobe diagrams for an HSLA steel and two plain carbon steels based on peel data (from [21]).

Figure 9 Plug size as a function of weld time at an electrode force of 210 kgf. (○) Specimen A, 4.19 kA; (◑) Specimen A, 3.4 kA; (□) Specimen B, 6.21 kA; (▣) Specimen B, 3.83 kA.

at 7.26 kA in Fig. 8 and 6.21 kA in Fig. 9, the plug size is nearly independent of the weld time.

It should be pointed out that Specimens B welded under the conditions of 7.26 kA, 290 kgf, and 6.21 kA, 210 kgf, exhibit expulsive failures, which are indicated by dotted lines in Figs 8 and 9. Because the plug size is measured with respect to the maximum average perpendicular direction of the specimen after the peel test, the as-evaluated plug diameter tends to be larger than that observed in the cross-sectional view as shown in Fig. 4a. Within the Lobe curve, especially the right portion region, the measured plug size may be larger than the original electrode-tip diameter. Nevertheless, the normal failure mode still prevails, and no splash is observed.

According to the study of Tatsumoto [23] on spot weldability of aluminium alloys, the relationship between contact resistance and electrode force is strongly dependent on the specimen surface condition. For specimens with surface pickled by acid or ground by SiC paper or brushed by steel fibre, the contact resistance is decreased as the electrode force is increased. However, for an untreated specimen, the contact resistance, exhibiting a very high value, is nearly independent of the electrode force. In this study, it is interesting to note that curves of plug size versus weld time for Specimen A exhibit identical slopes under various electrode forces, as shown in Figs 8 and 9. It appears that the effect of electrode force on the dependence of plug size on weld time is more substantial in Specimen B compared to Specimen A, which is consistent with the results of Tatsumoto [23].

The weld behaviour in the Fe–Al–Mn–Cr alloy system can be further appreciated in Fig. 10, in which the plug size is related to the weld current at a constant weld time of 10 cycles. It is observed that the plug size increases in proportion to the weld current and a nearly identical slope in the plug size–weld
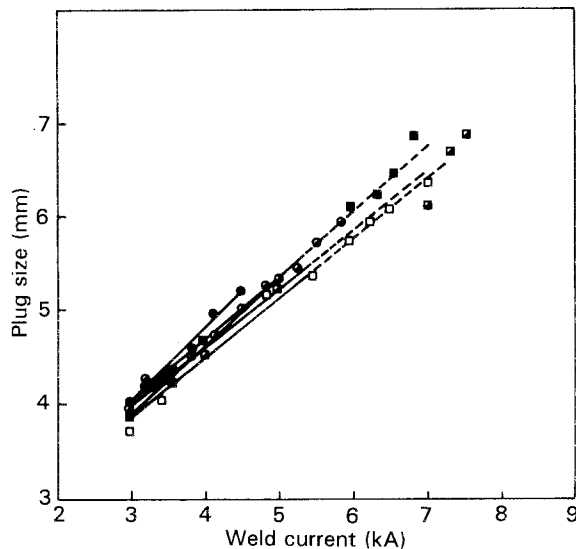
current dependence prevails under various weld conditions for electrode forces and surface treatments, except at constant weld time.

The relationships between indentation and weld time under different electrode force, surface condition, and weld current, are illustrated in Figs 11 and 12. The acceptable weld is represented by solid lines and the expulsive unacceptable weld by dots. In Fig. 11 it is seen that curves of indentation versus weld time at weld currents of 4.19 and 3.4 kA for Specimen A are nearly parallel. However, for Specimen B, the slope of indentation versus weld time curve is smaller than that for Specimen A. On the basis of Figs 11 and 12, it is apparent that the indentation increases with increasing electrode force. Nevertheless, the dependence of the indentation as a function of weld time is insignificant for Specimen B at lower weld current, such as the
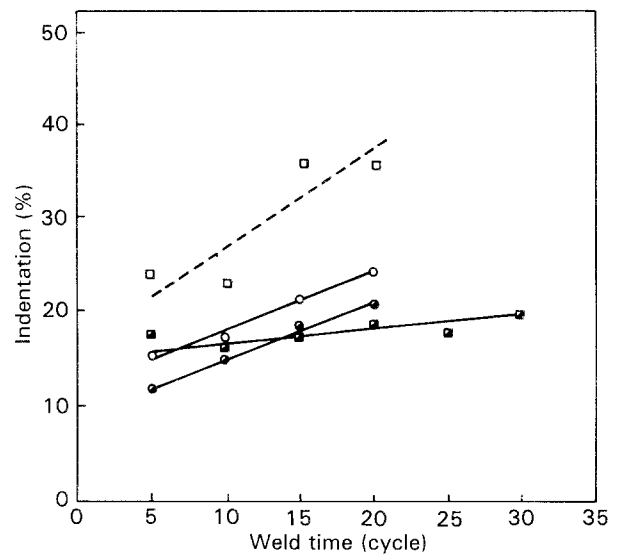

Figure 11 Indentation as a function of weld time at an electrode force of 290 kgf. (○) Specimen A, 4.19 kA; (◑) Specimen A, 3.4 kA; (□) Specimen B, 6.21 kA; (�◪) Specimen B, 3.83 kA.

Figure 10 Plug size as a function of weld current at a weld time of 10 cycles. (●) Specimen A, 290 kgf; (◑) Specimen A, 210 kgf; (▰) Specimen B, 290 kgf; (■) Specimen B, 210 kgf; (▢) Specimen B, 150 kgf.
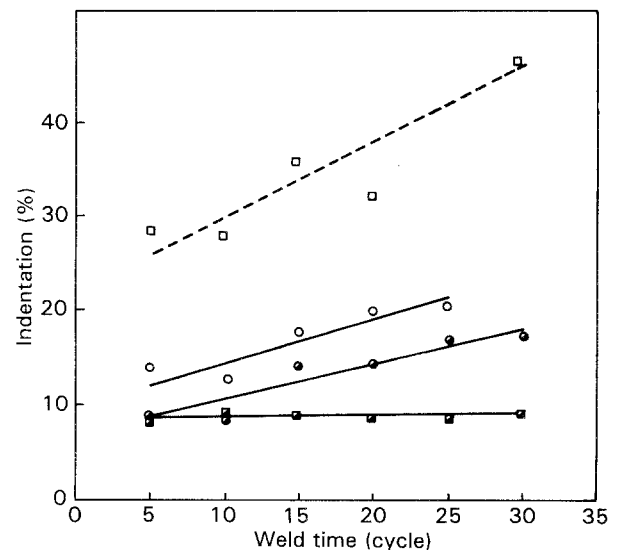

Figure 12 Indentation as a function of weld time at an electrode force of 210 kgf. (○) Specimen A, 4.3 kA; (◑) Specimen A, 3.4 kA; (□) Specimen B, 7.26 kA; (▪) Specimen B, 3.98 kA.
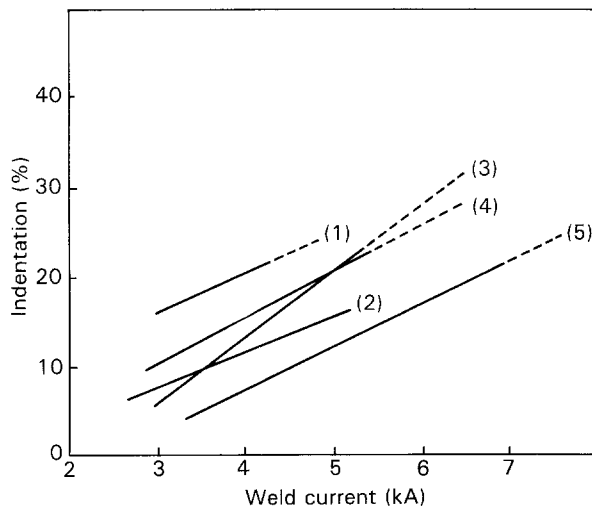
Figure 13 Indentation as a function of weld current at a weld time of 10 cycles. (1) Specimen A, 290 kgf; (2) Specimen A, 210 kgf; (3) Specimen B, 290 kgf; (4) Specimen B, 210 kgf; (5) Specimen B, 150 kgf.

cases of 3.83 kA, 290 kgf in Fig. 11 and 3.98 kA, 210 kgf in Fig. 12.

A further investigation of the effect of weld current on the indentation can be fulfilled on the basis of Figs 11 and 12. Fig. 13 presents the relationship between indentation and weld current at a weld time of 10 cycles. For both Specimens A and B under different electrode forces, the indentation increases as the weld current is increased. In summary, it is interesting to point out that the dependence of indentation on weld time and weld current are similar to that of plug size versus weld time and weld current, as indicated in Figs 8–10. The different surface treatment tends to affect the plug size and indentation dependence on weld time, but not on weld current under the conditions employed in this study.

4. Conclusions

1. The spot weldability of Fe–Mn–Al–Cr–C alloy is generally good. The acceptable weld currents range from 3.5–6 kA, which are lower than those of high-strength low-alloy steel and plain carbon steel.

2. The untreated specimen with α-Al_2O_3 on the surface exhibits narrower Lobe range than that of the acid-pickled specimen.

3. For the surface untreated specimen, the plug size is linearly proportional to the weld time. However, for the surface acid-pickled specimen, the dependence of plug size on the weld time is decreased as the electrode force is increased. For higher electrode force at 290 kgf, the plug is nearly independent of the weld time for the surface acid-pickled specimen.

4. The indentation is proportional to the weld current for Fe–Mn–Al–Cr–C alloys. The relationship between indentation and weld time depends on the surface condition and electrode force. For the untreated specimen, the indentation is linearly proportional to weld time within the Lobe region. In contrast, the dependence for the acid-pickled specimen is less significant compared to that of the untreated specimen.

References

1. S. K. BANERJI, Proceedings of the Workshop on "Conservation and Substitution Technology for Critical Materials", Vanderbilt University, Nashville, Tennessee, June 1981.
2. Idem, presented at the Public Workshop on "Trends in Critical Materials Requirements for Steels of the Future-Conservation and Substitution Technology for Chromium", Vanderbilt University, Nashville, Tennessee, October 1982.
3. J. P. SAUER, R. A. RAPP and J. P. HIRTH, Oxid. Metals 18 (1982) 285.
4. C. J. WANG and J. G. DUH, J. Mater. Sci. 23 (1988) 769.
5. J. G. DUH, J. W. LEE and C. J. WANG ibid. 23 (1988) 2649.
6. C. J. WANG and J. G. DUH, ibid. 23 (1988) 2913.
7. Idem, ibid. 23 (1988) 3447.
8. J. G. DUH and J. W. LEE, J. Electrochem. Soc. 136 (1989) 847.
9. J. G. DUH and C. J. WANG, J. Mater. Sci. 25 (1990) 268.
10. Idem. ibid. 25 (1990) 2063.
11. Idem. ibid. 25 (1990) 2615.
12. C. P. CHOU and C. H. LEE, ibid. 25 (1990) 1491.
13. Idem, J. Mater. Sci. Eng. A 118 (1989) 137.
14. Idem, Scripta Metall. A 23 (1989) 901.
15. JIS Z3136, "Method of Tension Shear Test for Spot Welded Joint" (Japanese Standards Association, Tokyo, 1988).
16. D. W. DICKISON, in Report on AISI Project No. 1201–409C, "Welding In the Automotive Industry State of the Art" (AISI, June 1986) p. 180.
17. AWS document D8. 7-78 (SAE HSJ1188), "Specification for Automotive Weld Quality- RSW" (American Welding Society, 1978).
18. JIS Z3140, "Method of Inspection for Spot weld" (Japanese Standards Association, Tokyo, 1988).
19. W. F. HESS, W. D. DOTY and W. J. CHILDS, Weld. J. 26 (1947) 583s.
20. I. W. JOHNSON, ibid. 39 (1960) 89s.
21. J. M. SAWHILL Jr and S. T. FURR, Soc. Automotive Eng. (Society of Automotive Engineers, Warrendale, PA) (1982) 1462.
22. W. A. TILLER and J. W. RUTTER, Canad. J. Phys. 34 (1956) 96.
23. T. TATSUMOTO, Weld. Tech. (Jpn) 24 (2) (1976) 57.